Influence of Cationic Vacancies and Hydrostatic Pressure on Electronic and Magnetic Properties of Doped ZnTe:Mn Crystal

S.V. Syrotyuk*

Lviv Polytechnic National University, 12 S. Bandera Str., 79013 Lviv, Ukraine

Doi: 10.12693/APhysPolA.141.333   *e-mail: svsnpe@yahoo.com

The influence of hydrostatic pressure and cationic vacancies on the electronic and magnetic properties of the ZnTe:Mn crystal is investigated. First-principles calculations have been carried out for the supercell $2 \times 2 \times 2$, containing 64 atoms, using the ABINIT code. The hybrid exchange–correlation functional PBE0 was used to correctly describe the strongly correlated $3d$-electron subsystem. The Hamiltonian matrix was calculated on the one-electron basis of the projector augmented waves. At the first stage, the calculations were performed in the ambient and compressed states of the material. In the second stage, we have evaluated the electronic properties in the ZnTe:Mn material taking into account the simultaneous effect of the cationic vacancies and the hydrostatic pressure. It was found that for both uncompressed and compressed states of the material, the introduction of the cationic vacancies leads to its transition to the metallic state. A significant influence of the cationic vacancies on the value and nature of the resulting magnetic moment of the supercell was also revealed. Based on the results obtained in this paper, an assumption is made about a non-collinear model of magnetism in the material caused by cationic vacancies.

topics: DFT, strong correlation, electronic properties, pressure effect

1. Introduction

ZnTe is one of the promising materials for potential photovoltaic applications, namely in solar cells, photodiodes and LEDs. The large energy band gap, low resistivity and high visible range transparency of the ZnTe are used in a variety of microelectronic and optoelectronic devices [1]. The ZnTe doped with Cu shows a significant decrease in resistance and increase in mobility of carriers. The decrease in resistivity and the high transmission are complementary factors regarding the efficient application of the material in optoelectronic devices.

The doping of the ZnTe crystal is performed in order to improve the electrical and optical properties. This has led to an increase in interest in the alloying of this material, in particular with 3d transition elements. For example, ZnTe doped with Cr can provide broadly tunable radiation with high efficiency in the mid-IR spectra region (2–3 μm) [2]. The material ZnTe:V shows the improved photorefractive response from 0.6 to 1.3 μm, having attractive applications of optical power limiting, holographic interferometry, and optical communicating [2].

In work [3], the optoelectronic and transport features of the ZnTe:Mn ($x = 8\%$ and $x = 16\%$) crystals have been simulated within the DFT approach using the GGA+U approximation. It was shown that the materials studied are semiconductors with a direct type band energy gap (G–G) with magnitudes equal to 2.20 eV and 2.0 eV for ZnTe:Mn $x = 8\%$ and $x = 16\%$, respectively. The calculated dispersions of optical functions within the energy range of 0–25 eV show that the up states of 8 and 16% possess strong optical response in the energy range covering the visible light and extreme UV regions. Thus, the direct band gap and strong absorption in this region of energy make these materials excellent candidates for optoelectronic devices. Based on the transport kinetics calculations, we have also shown that both ZnTe:Mn ($x = 8\%$ and $x = 16\%$) crystals show promising thermoelectric properties.

The objective of the present work is to investigate the electronic structure of the ZnTe:Mn material using the first-principles projector augmented wave (PAW) approach [4]. The electronic structure is evaluated at ambient conditions and under hydrostatic pressure, with and without the cationic vacancies at the Zn atom sites.

The remainder of the paper is organized as follows: Sect. 2 describes the calculation method, Sect. 3 presents the results and a discussion of the electronic and finally, Sect. 4 summarizes the conclusions of this work.

2. Computational details

PAW [4, 5] approach combines features of the pseudopotential and the full-potential linearized augmented plane waves (FP-LAPW) methods. The all electronic wave function $|\psi_n(\boldsymbol{r})\rangle$ is obtained by the action of the τ operator on the pseudo-wave function $|\tilde{\psi}_n(\boldsymbol{r})\rangle$, i.e.,

$$|\psi_n(\boldsymbol{r})\rangle = \tau |\tilde{\psi}_n(\boldsymbol{r})\rangle, \qquad (1)$$

where

$$\tau = 1 + \sum \sum \left(|\phi_i^a(\boldsymbol{r})\rangle - |\tilde{\phi}_i^a(\boldsymbol{r})\rangle \right) \langle \tilde{p}_i^a|. \qquad (2)$$

Here $|\phi_i^a(\boldsymbol{r})\rangle$ is an atomic wave function, $|\tilde{\phi}_i^a(\boldsymbol{r})\rangle$ is a pseudowave function, and $\langle \tilde{p}_i^a|$ is a projector function. Summation in (2) is carried out over augmentation spheres, which are numbered with index a, and the index $i = \{n, l, m\}$ corresponds to the quantum numbers. Substituting the all-electron function defined by (1) into the Schrödinger equation

$$H|\tilde{\psi}_{n\boldsymbol{k}}\rangle = |\psi_{n\boldsymbol{k}}\rangle \varepsilon_{n\boldsymbol{k}}, \qquad (3)$$

we obtain the transformed equation

$$\tau^+ H \tau |\tilde{\psi}_{n\boldsymbol{k}}\rangle = \tau^+ \tau |\tilde{\psi}_{n\boldsymbol{k}}\rangle \varepsilon_{n\boldsymbol{k}} \qquad (4)$$

having identical electronic energy band spectrum $\varepsilon_{n\boldsymbol{k}}$ as in (3). Here n denotes the band number, and $\boldsymbol{k}$ is a vector from the first Brillouin zone.

The exchange–correlation energy functional was used in the hybrid form of PBE0 [6]. The latter includes a usual GGA-PBE exchange–correlation functional [7] and the Hartree-Fock exchange term E_x^{HF} of the 3d electrons, which is self-interaction free, i.e., it partly removes the self-interaction error (SIE) from the exchange–correlation functional. The use of the PBE0 functional allows obtaining better values of the eigenenergies for 3d states and more accurate values of the band gap for the materials ZnS:Cr:Fe [7], ZnSe:Cr [8], and for half-Heusler alloy MnCoSi [9].

The valence basis states used for PAW generation have been selected as follows: $4s^2 3d^{10}$ for Zn, $3s^2 3p^6 4s^2 3d^5$ for Mn, and $5s^2 5p^4$ for Te. All the PAW basis functions were obtained using the program AtomPAW [10]. The radii of the augmentation spheres r_{PAW} are 1.8, 1.7, and 2.3 a.u. for Zn, Mn, and Te, respectively. The electronic energy bands have been evaluated by means of the ABINIT code [11, 12]. Integration over the Brillouin zone was performed on the Monkhorst–Pack [13] grid of $6 \times 6 \times 6$.

3. Results and discussions

The results of the electronic structure calculations for the material ZnTe:Mn are shown in Figs. 1–8. Figure 1a, b shows the electron energy spectrum for electrons with spin up and down, respectively, obtained in the absence of external hydrostatic pressure ($P = 0$). Optical and fundamental gaps for both spin orientations are the same and
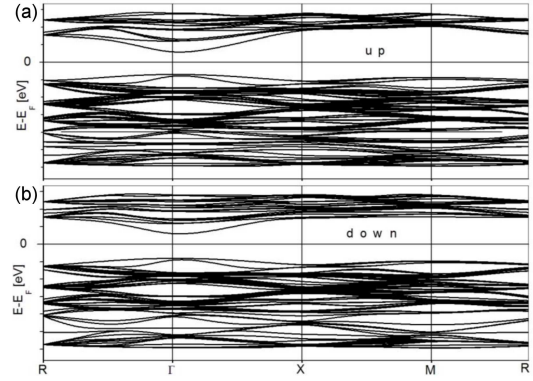

Fig. 1. The spin-polarized energy band structure of the ZnTe:Mn material obtained at ambient pressure, without the cationic vacancies.
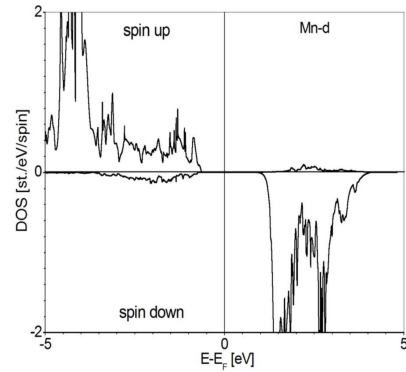

Fig. 2. The electronic DOS of the ZnTe:Mn material obtained at ambient pressure, without the cationic vacancies.

equal to 1.05 and 1.18 eV, respectively. The Fermi level is located approximately in the middle of the forbidden gap.

Figure 2 shows the 3d density of states of the Mn electrons. The value of the direct gap E_g at point Γ is 1.03 eV for the spin up and 1.18 eV for the spin down. We see that the density of states (DOS) curves show a significant asymmetry about the energy axis. The consequence of this is a non-zero magnetic moment of the supercell, which is equal to 5 μ_{B} (Bohr magneton). This value is formed by the charge within the atomic Mn sphere (3.82 μ_{B}), and other atoms contribute only a value of 0.1 μ_{B}. The contribution to the magnetic moment of electrons localized in the interspherical region is 1.08 μ_{B}.

The effect of the Zn vacancies can be detected from the dependencies shown in Figs. 3 and 4. Figure 3a shows that for the spin up, the Fermi level is immersed in the upper part of the valence band due to the presence of the cationic vacancies in the material. Figure 3b shows that for the spin down, the Fermi level is also immersed in the upper part of the valence band, which is also due to the cationic vacancies in the material.
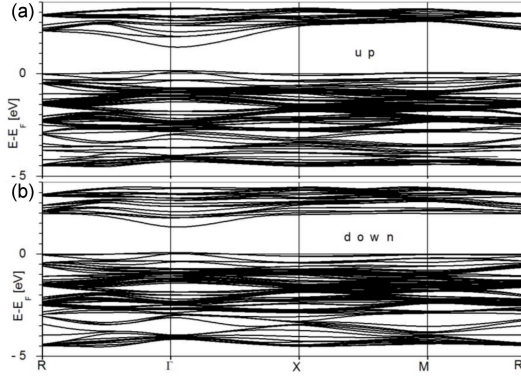
Fig. 3. The spin-polarized energy band structure of the ZnTe:Mn material obtained at ambient pressure, with the cationic vacancies.
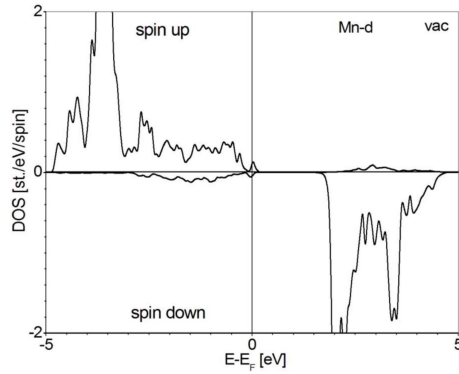

Fig. 5. The spin-polarized energy band structure of the ZnTe:Mn material obtained at pressure $P = 47$ GPa, without the cationic vacancies.

Fig. 4. The electronic DOS of the ZnTe:Mn material obtained at ambient pressure, with the cationic vacancies.

Fig. 6. The electronic DOS of the ZnTe:Mn material obtained at pressure $P = 47$ GPa, without the cationic vacancies.

The magnetic moment of the supercell is 4.57 μ_B. This value is formed by the charge of the atomic Mn sphere (3.81 μ_B), and other atoms contribute a negative value (-0.13 μ_B), i.e., the atomic spheres provide the value of the magnetic moment 3.68 μ_B. The contribution to the magnetic moment of electrons localized in the interspherical region is 0.89 μ_B.

A comparison of Figs. 2 and 4 shows that the Fermi level shifts downward in electron energy and is located in the upper part of the valence band (see Fig. 4). This change is due to the presence of the Zn atom vacancies, i.e., cationic vacancies. In a crystal without vacancies (see Figs. 1, 2), we operate with the concept of interband gap. Then we characterize the material with the vacancies using a pseudo-gap because the Fermi level is localized in the valence band. The value of the direct pseudo-gap at point Γ is 1.03 eV for the spin up states, and 1.14 eV for the spin down states, respectively.

The effect of pressure in the material without the vacancies can be detected by comparing Figs. 1 and 5, as well as Figs. 2 and 6. In Fig. 5 it can be seen that for the spin up states, the Fermi level is slightly shifted to the valence band, and for the
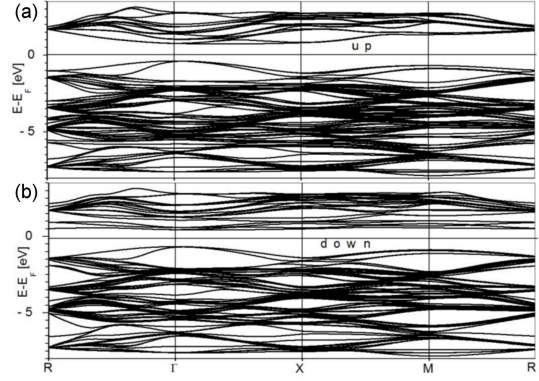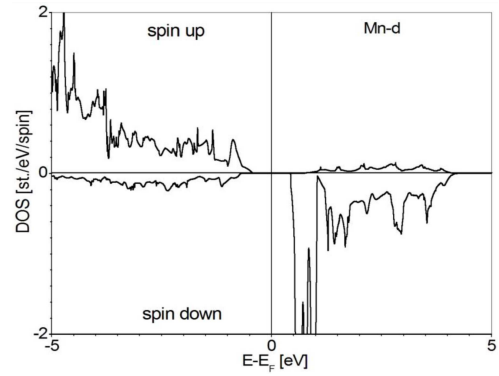
spin down states, it is localized closer to the conduction band. For both spin orientations, the compressed material is a semiconductor with fundamental indirect (Γ–X) gap of 1.10 eV for electrons with spin up, and 1.09 eV for electrons with spin down, and the corresponding optical gaps equal to 1.12 and 1.09 eV, respectively.

Figure 6 also shows a noticeable redistribution of DOS 3d electrons Mn. The total magnetic moment of the supercell is 5 μ_B. It is formed by charges inside the attachment sphere of the Mn atom (3.62 μ_B) and other atomic spheres (0.44 μ_B), which together is equal to 4.06 μ_B. The contribution of the interspherical region of the entire supercell is 0.94.

The following two Figs. 7 and 8 reveal the combined effect of the pressure and vacancies on the parameters of the electronic energy band spectrum of the material. Comparing Fig. 7a and Fig. 7b, we see that for electrons with spin up, the Fermi level is more immersed in the valence band than for carriers with the opposite spin moment. The value of the pseudo-gap for the spin up is 1.09 eV, and for the spin down it is less and equals 0.84 eV. Significant asymmetry of DOS, shown in Fig. 8, indicates
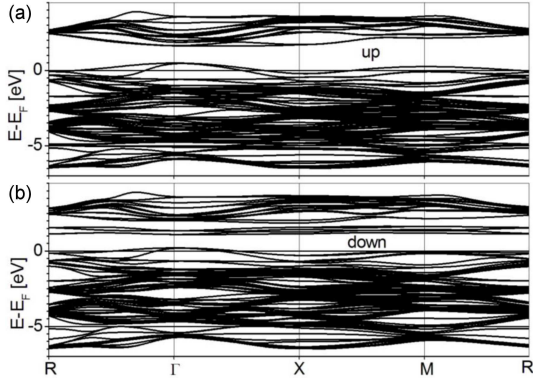
Fig. 7. The spin-polarized energy band structure of the ZnTe:Mn material obtained at pressure $P = 44$ GPa, with the cationic vacancies.
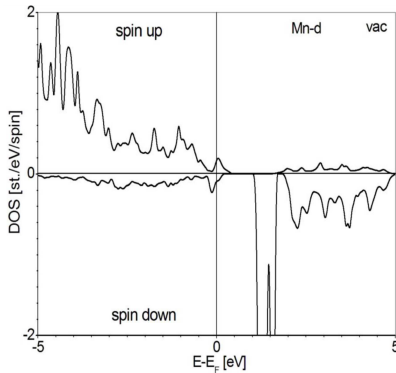

Fig. 8. The electronic DOS of the ZnTe:Mn material obtained at pressure $P = 44$ GPa, with the cationic vacancies.

a non-zero magnetic moment of the supercell, which is equal to 4.12 μ_B. This value was formed by electrons inside the augmentation sphere of the Mn atom (3.58 μ_B). In fact, the total magnetic moment of the spheres of other atoms, which equals -0.13 μ_B, opposes this value. Thus, all atomic spheres in the supercell produce a magnetic moment of 3.45 μ_B, and the interspherical density of electrons causes a magnetic moment of 0.67 μ_B. The last two of the mentioned values give the magnetic moment of the supercell of 4.12 μ_B.

4. Conclusions

The results of the calculations allow us to identify the following important moments of the influence of the pressure and cationic vacancies on the parameters of the electronic structure of the doped ZnTe:Mn crystal.

1. The compressed ZnTe:Mn material exhibits semiconductor properties for both spin orientations. Hydrostatic pressure causes a small increase in the band gap for electrons with spin up and a slight decrease for electrons with spin down.

2. The magnetic moment of the supercell in the normal state and under the action of pressure is the same and equals 5 μ_B, although the corresponding contributions from the Mn atomic sphere are different and equal to 3.82 μ_B and 3.62 μ_B, respectively.

3. The presence of the cationic vacancies leads to a significant change in the properties of the material. Immersion of the Fermi level indicates that the material acquires metallic properties. In a compressed material with cationic vacancies, the immersion of the Fermi level in the valence band is much greater than in the uncompressed one.

4. If in the material without vacancies, the resulting magnetic moment of atomic spheres is added to that on the Mn atom, then in the presence of cationic vacancies, it will be subtracted, i.e., will reduce the magnetic moment of the supercell, which is 4.56 μ_B and 4.12 μ_B in uncompressed and compressed states, respectively.

5. The presence of the cationic vacancies leads to a change in the nature of magnetism of the material, i.e., in the material without the vacancies, it is collinear, and in the material with the vacancies, the magnetism is spiral. External hydrostatic pressure leads to a significant reduction in the magnetic moment of the supercell.

References

[1] W.A. Syed, S. Ahmed, M.S. Saleem, N.A. Shah, *Chalcogenide Letters* **12**, 215 (2015).

[2] B. Xiao, M. Zhu, B. Zhang, J. Dong, L. Ji, H. Yu, X. Sun, W. Jie, Y. Xu, *Optical Materials Express* **8**, 431 (2018).

[3] W. Khan, S. Azam, I. Ullah, M. Rani, A. Younus, M. Irfan, P. Czaja, I.V. Kityk, *Crystals* **9**, 247 (2019).

[4] P.E. Blöchl, *Phys. Rev. B* **50**, 17953 (1994).

[5] M. Torrent, F. Jollet, F. Bottin, G. Zerah, X. Gonze, *Comput. Mat. Science* **42**, 337 (2008).

[6] E. Tran, P. Blaha, K. Schwarz, P. Novák, *Phys. Rev. B* **74**, 155108 (2006).

[7] S.V. Syrotyuk, *J. Nano- Electron. Phys.* **13**, 05027 (2021).

[8] S.V. Syrotyuk, M.K. Hussain, *Phys. Chem. Solid State* **22**, 529 (2021).

[9] S.V. Syrotyuk, *Metallofiz. Noveishie Tekhnol.* **43**, 541 (2021).

[10] A.R. Tackett, N.A.W. Holzwarth, G.E. Matthews, *Computer Phys. Comm.* **135**, 348 (2001).

[11] X. Gonze, B. Amadon, P.-M. Anglade et al., *Computer Phys. Comm.* **180**, 258 (2009).

[12] X. Gonze, F. Jollet, F. Abreu Araujo et al., *Computer Phys. Comm.* **205,** 106 (2016).

[13] H.J. Monkhorst, J.D. Pack, *Phys. Rev. B* **13**, 5188 (1976).